

---

Chapter II  
Preparation and characterization

---

## SECTION A - PREPARATION

### 2.0 INTRODUCTION

The properties of ferrites are both intrinsic as well as sensitive structure. The extrinsic properties can be controlled with the help of the control over the preparation technique. The porosity, impurity and grain size mostly affect the extrinsic properties of ferrites. The purity, chemical homogeneity, stoichiometry, grain size etc also need to be controlled while preparing the ferrites. In this section different methods of ferrite preparation are discussed briefly.

### 2.1 METHODS OF FERRITE PREPARATION

#### 2.1.1 Ceramic Method

Ceramic method is one of the most extensively used method for ferrite preparation. High purity oxides of divalent transition metals and iron oxide are mixed in the required proportions in the wet medium. The dried mixture is presintered at a certain temperature (around 800 °C) for a few hours. The material is broken up, milled and sieved before pressing it in the desired form. The final sintering of the product is carried out at a suitable high temperature (1000 - 1200 °C).

### 2.1.2 Decomposition Method

The salts of metals like carbonates, nitrates and oxalates are sometimes used in place of oxides. At the time of sintering in air, they produce oxides by thermal decomposition. The oxides so formed consequently undergo solid state reaction to form a ferrite.

### 2.1.3 Hydroxide Precipitation Method

The method is based upon simultaneous precipitation of required oxides from solution. The essential requirements of the method are knowledge of solubility product and quantitative understanding of the chemical process. Economus [1] and Wolf et. al. [2] have employed this method for ferrites and rare earth garnets respectively.

### 2.1.4 Oxalate Precipitation Method

This method is preferred to others mainly because of the fact that ammonium oxalate does not leave any residue during precipitation. Secondly, most of metal oxalates are very similar in crystal structure so that precipitation tends to produce mixed crystals which contain the metallic cations in the proportion in which they were present in the solution. The mixing on the

molecular scale will lead to the formation of ferrite at much lower temperatures than those required for usual oxide mixtures.

## 2.2 SINTERING

The sintering process plays the important role in controlling the extrinsic properties of ferrites. The sintering is carried out generally in two stages.

### 2.2.1 Presintering

During presintering the materials react partially to form a ferrites. The purpose of presintering is -

- 1) to decompose the carbonates or higher oxides thereby reducing the evolution of gas in the final sintering
- 2) to assist in homogenizing the materials
- 3) to reduce or control the shrinkage occurring during final sintering.

### 2.2.2 Final Sintering

The final sintering is the vital part in ceramic process. At the time of the final sintering, development of microstructure starts. This sintering is carried out at high temperature above 1000 °C. With a proper control over sintering temperature and time one

can develop ferrites having desired grain size and porosity.

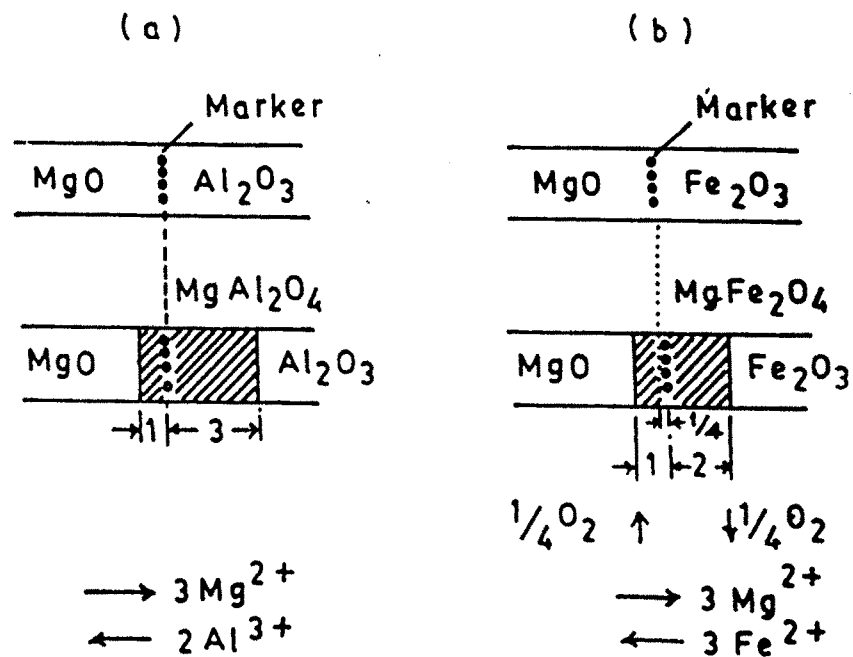
The rate at which the ferrite are cooled also affect the magnetic properties of ferrites. The cooling rate must be slow to avoid brittle solids and random distribution of ions on A and B sites. The ferrites are required to be cooled in low oxygen atmosphere to avoid re-oxidation of ferrite which results in the formation of non-magnetic surface layer.

\*  
explain.

### 2.2.3 Solid State Reaction

According to Wagner [3] the spinel phase  $Mg^{2+}Fe_2^{3+}O_4$  is formed at the interface of  $MgO^{2+}$  and  $Fe_2^{3+}O_3$ . The reaction proceeds by the counter diffusion of the cations  $Mg^{2+}$  and  $Fe^{3+}$  in the ratio 3:2 through a practically rigid lattice of oxygen anions (Figure 2.1 a). If we provide the interface with marker in the ratio 1:3 the marker should be undergo no shift during the reaction. The ratio for  $MgAl_2O_4$  is found to be 1:3 where as it is 1:2.7 for  $MgFe_2O_4$  [4].

According to the Wagner model, in case of  $MgAl_2O_4$  formation, the  $Fe_2O_3$  of  $MgFe_2O_4-Fe_2O_3$  phase boundary dissolves into the spinel phase without any loss of oxygen i.e. iron remains in the trivalent state. The



a) Counter diffusion of Mg<sup>2+</sup> and Al<sup>3+</sup> cations, no anion diffusion (Wagner mechanism).

b) Counter diffusion of Mg<sup>2+</sup> and Fe<sup>2+</sup> cations, no O<sup>2-</sup> anion diffusion but reduction and oxidation of Fe ions at the respective phase boundaries which is equivalent to an oxygen transport through the gas phase.

Fig. 2·A·2 — MECHANISMS OF THE FORMATION OF  
a) MgAl<sub>2</sub>O<sub>4</sub> AND b) MgFe<sub>2</sub>O<sub>4</sub>.

dissolution of  $\text{Fe}_2\text{O}_3$  into spinel is accompanied by the loss of oxygen. Assuming counter diffusion model with  $\text{Mg}^{2+}$  and  $\text{Fe}^{2+}$  instead of  $\text{Mg}^{2+}$  and  $\text{Fe}^{3+}$  and with oxygen transport through the gas phase the volume ratio of  $\text{MgFe}_2\text{O}_4$  phase formed on both side of markers should be 1:2 and there should be smaller displacement of the markers. The effect is also called as Kirkendall effect (Figure 2.1b). This mechanism has the important consequence that the reaction becomes dependent on oxygen partial pressure. The reaction rate will increase by reducing conditions because large concentration gradient are set-up over the reaction layer and more  $\text{Fe}_2\text{O}_3$  can dissolve into the spinel phase [5]. It is proved earlier [6] that the formation of  $\text{MgFe}_2\text{O}_4$  takes place due to Kirkendall effect. The completion of solid state reaction can be confirmed by x-ray diffraction technique.

#### 2.2.4 HOT PRESSING

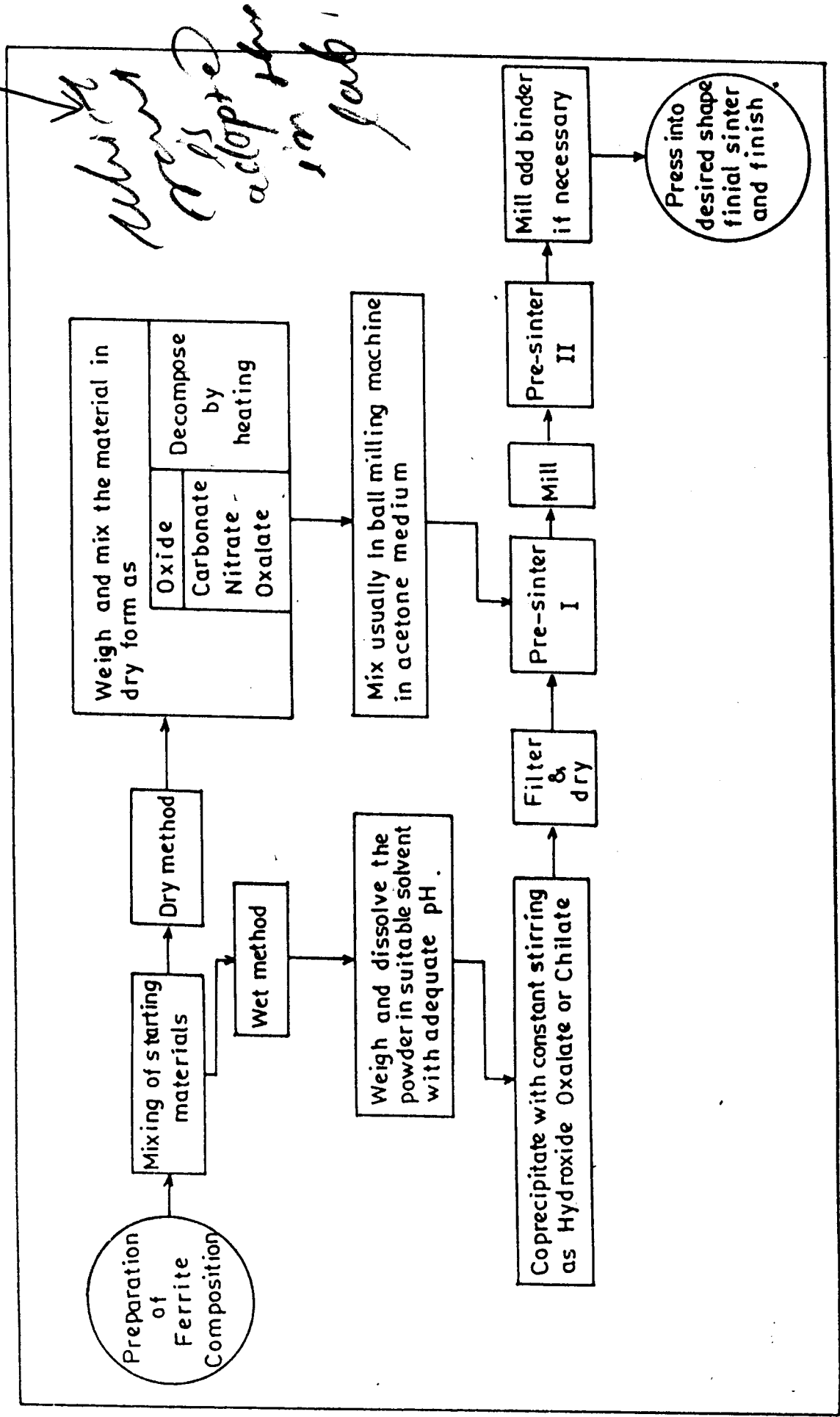
To achieve the small grain size and high density usually hot pressing technique is used. In this process, simultaneous application of temperature and pressure take place [7]. The powder is enclosed in a flexible container of rubber or plastic which may be

evacuated and is compacted by immersing the container in an oil bath to which the pressure is applied. This effect is to give much more uniformity and high density than the conventional methods. It also encourages continuous grain growth and favours to obtain low porosity and grain size. It seems apparent that pressure should lead to a high degree of compaction and enhance contact between grains during sintering. At 1000°C ferrites have sufficient plasticity to flow to a considerable extent at high pressures. It is favourable to produce high density compacts in which the original grain size is maintained. Hot pressing method is explained in detail by Murray et al [7] and extended by Oudemans et al [8].

### 2.3 PREPARATION OF FERRITE SAMPLES (PRESENT CASE)

Ceramic technique involving double sintering was used in the present case. In the ferrite system  $Zn_xMg_{1-x-t}Ti_tFe_{2-2t}O_4$  where  $x = 0.3$ ,  $t = 0, 0.05, 0.1, 0.2$  and  $t = 0.05$ ,  $x = 0.2, 0.3, 0.4, 0.6$  eight samples were prepared. High purity oxides of zinc, magnesium, titanium and iron were weighed in desired proportions and mixed physically in agate mortar in acetone medium. The presintering was carried out at 700 °C for eight

Fig 2.2 - FLOW CHART OF STAGES IN PREPARATION OF FERRITE BY CERAMIC METHOD IN LAB.



hours. The temperature of furnace was measured with the help of chromel alumel thermocouple which was calibrated before measuring the temperature of the furnace. The presintered powder was then ground in the agate mortar in acetone medium. The pellets were prepared by pressing the powder in a die of 1 cm diameter with the help of hydraulic press by applying pressure of about 7 to 8 tons per square inch for 3 minutes. Toroids were also prepared with the help of toroid die. The final sintering of the compacts was carried out at 1100 °C for 40 hours in air medium. The furnace was cooled at the rate of 80 °C per hour. The flow chart of preparation of ferrites is shown in the Figure 2.2.

## SECTION - B : X-RAY STUDIES

### 2.4 INTRODUCTION

X-ray diffraction has an important role in research on solids in general and crystals in particular. With the help of x-ray diffraction one can determine -

- 1) the crystallinity of a given solid and its crystal structure,
- 2) the nature of the phases present and

3) structural parameters like lattice constant, interplaner distances, radii of octahedral and tetrahedral interstices and bond lengths.

According to Bragg's law, x-rays are diffracted from the planes (h k l) when the equation

$$2d_{(hkl)} \sin \theta = n\lambda \quad \dots \quad 2.1$$

where n - order of reflection d - interplaner distance for (hkl) planes and  $\theta$  - glancing angle satisfied.

One can scan the diffraction pattern of the crystal either by varying the wavelength ( $\lambda$ ) or by varying glancing angle ( $\theta$ ). Diffraction methods have been developed to accomplish this. Depending on the experimental situation the methods of diffraction are as follows -

#### 2.4.1 Laue Method

In this method the crystal is kept stationary in a beam of continuous x-rays. The crystal selects a suitable wavelength ( $\lambda$ ) and diffraction occurs from a plane with incident glancing angle ( $\theta$ ).

#### 2.4.2 Rotating Crystal Method

In this method a crystal is rotated about a fixed axis in a beam of x-rays having fixed wavelength. For a particular value of  $\theta$  Bragg's law is satisfied and diffraction occurs.

#### 2.4.3 Powder Method

This is the most widely used method of x-ray diffraction of polycrystalline samples. This method was developed by Debye and Scherrer [9] and Hull [10]. In this method the fine grained powder is filled in a capillary tube. The diffraction occurs simultaneously from the individual crystallites that happen to be oriented with planes having the same angle of incidence  $\theta$ . In this method the wavelength is fixed and crystal is rotated. Recently, the counter diffractometers have been developed to record the diffractograms. In the counter diffractometer, the sample is placed at the center, so that x-rays fall on the plane surface of the sample. About the same axis, rotates an arm carrying a Geiger counter which records the diffracted x-rays. When the sample is rotated by an angle  $\theta$ , the counter is turned through  $2\theta$ . After complete scanning the XRD machine gives a record showing the variation of

intensities of diffracted  
x-rays with angle  $\theta$ .

## 2.5 RELEVANCE OF X-RAY DIFFRACTION TO FERRITE RESEARCH

In as much as most of the ferrites are synthesized by ceramic method and chemical method, it is almost essential to verify the formation of the ferrite. The degree of crystallinity also needs to be found out and the structural parameters like lattice constant, position parameter and bond lengths need to be determined. However the composition of the ferrite affects these structural parameters to a lesser extent. But the cation distribution is very much sensitive to composition and which gives rise to drastic change in magnetic properties of ferrite. Therefore, it is but natural to look towards X-ray diffraction as an important and indispensable tool to study the distribution of cations over the available sites in the spinel structure.

Notwithstanding the above, it is sometimes essential to differentiate between the transition metal cations having nearly the same atomic scattering factor for x-rays. In such a situation neutron diffraction has to be used as a complementary tool. As the element that

differ by only one atomic number, neutron diffraction can show well distinguished lines due to the net magnetic moment interacting with the neutron magnetic moment. Neutron diffraction studies have been used to find out the occupancy of different sites as well as the oxygen parameters and magnetic orientation of the magnetic moments of the ions. The neutron diffraction studies of ferrites were carried out by number of workers including Shull and Hastings [11,12]. Information about the particle size of the ferrites can be obtained from x-ray line widths [13].

The present study of diffraction is used to confirm the completion of solid state reaction, observe impurity phases and to determine the structural parameters.

## 2.6 EXPERIMENTAL TECHNIQUES

The powder diffraction patterns of all samples studied in the present case were recorded with the help of computerized XRD unit (Philips Model- APD 1710) with  $\text{CuK}\alpha$  radiation ( $\lambda = 1.5418 \text{ \AA}$ ) at USIC, Shivaji University, Kolhapur. The x ray diffraction patterns were taken with  $2\theta$  values ranging between  $20^\circ$  to  $80^\circ$  at a chart speed of  $2^\circ/\text{min}$ .

## 2.7 RESULTS AND DISCUSSION

The x-ray diffraction patterns for the  $Ti^{4+}$  substituted Mg-Zn ferrites viz.  $Zn_xMg_{1-x+t}Ti_tFe_{2-2t}O_4$  where  $x = 0.3$ ,  $t = 0, 0.05, 0.1$  and  $0.2$  and  $x = 0.05$ ,  $x = 0.2, 0.3, 0.4, 0.6$ , are shown in Figures 2.3 to 2.10. The diffraction patterns were indexed in the light of the crystal structure of natural spinel. The calculated and observed 'd' values are given in Tables 2.1 to 2.8. It is seen that the calculated and observed d values are in good agreement with each other for all indexed planes. Since diffraction patterns do not show any extra lines, single phase ferrite formation is confirmed.

The variation of the lattice parameter with content of titanium (t) is shown in Figure 2.11a. It is seen that there is an increase in the value of lattice parameter with  $Ti^{4+}$  concentration. Das et al [14] have studied the influence of  $Ti^{4+}$  in Ni-Zn ferrites. They have reported that lattice parameter initially decreases while after particular  $Ti^{4+}$  concentration there is monotonic increase in 'a' with the increase of  $Ti^{4+}$  concentration. Usha-Varshney et al [15] have reported variation of lattice parameter with the

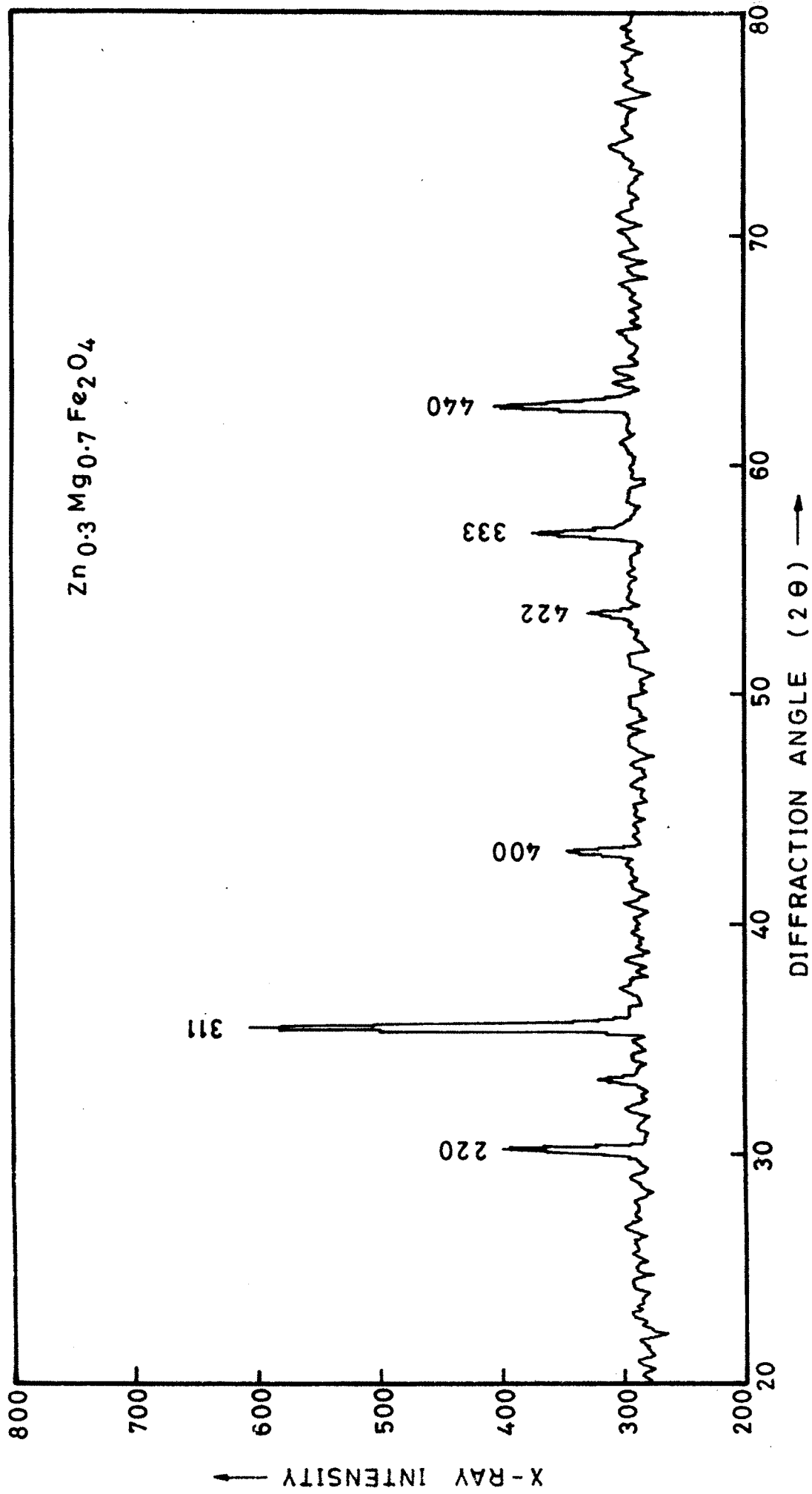


FIG. 2.3-X-RAY DIFFRACTION PATTERN OF  $Zn_{0.3}Mg_{0.7}Fe_2O_4$ .

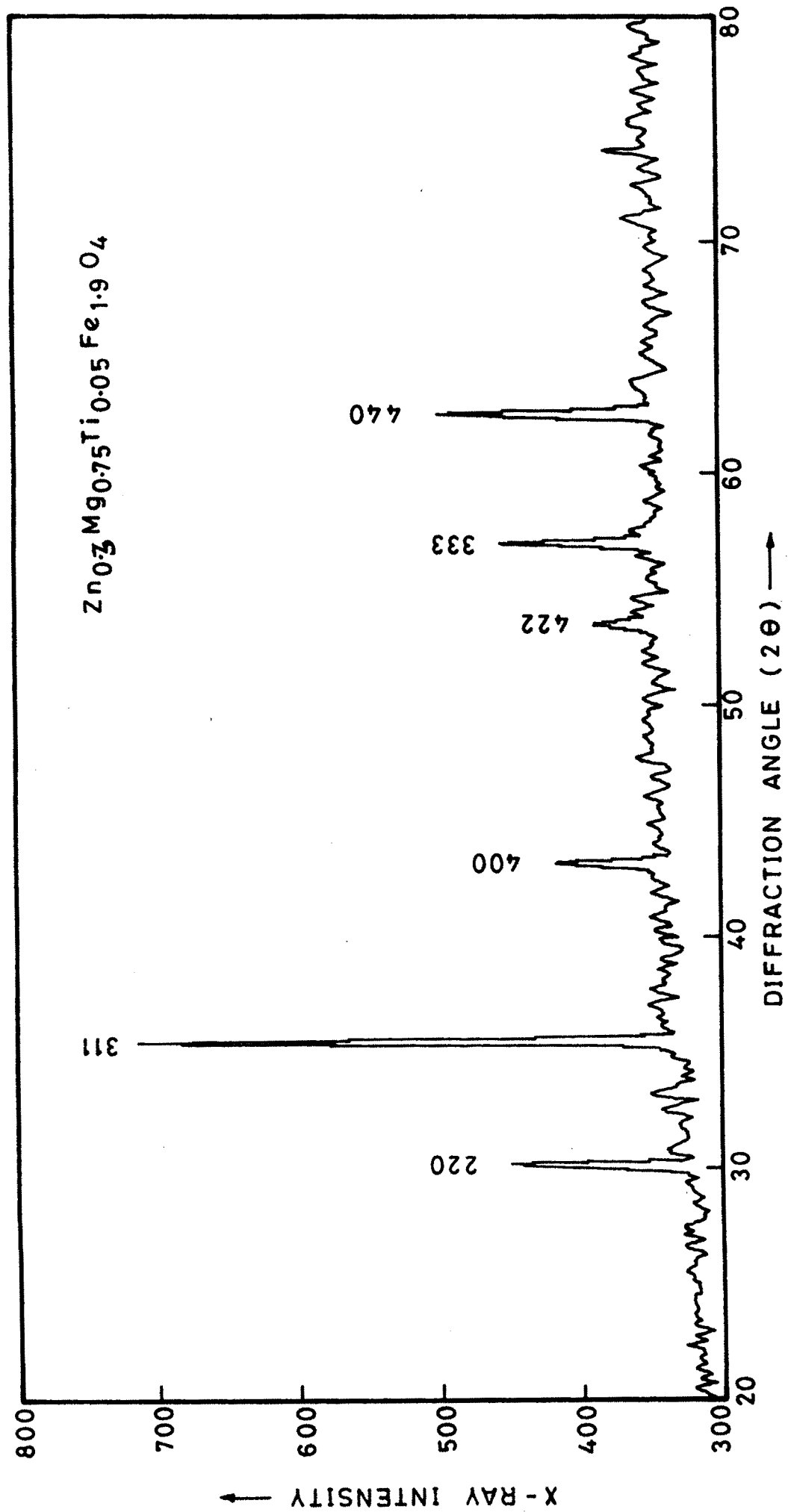


FIG. 2.4 - X-RAY DIFFRACTION PATTERN OF  $Zn_{0.3}Mg_{0.75}Ti_{0.05}Fe_{1.9}O_4$ .

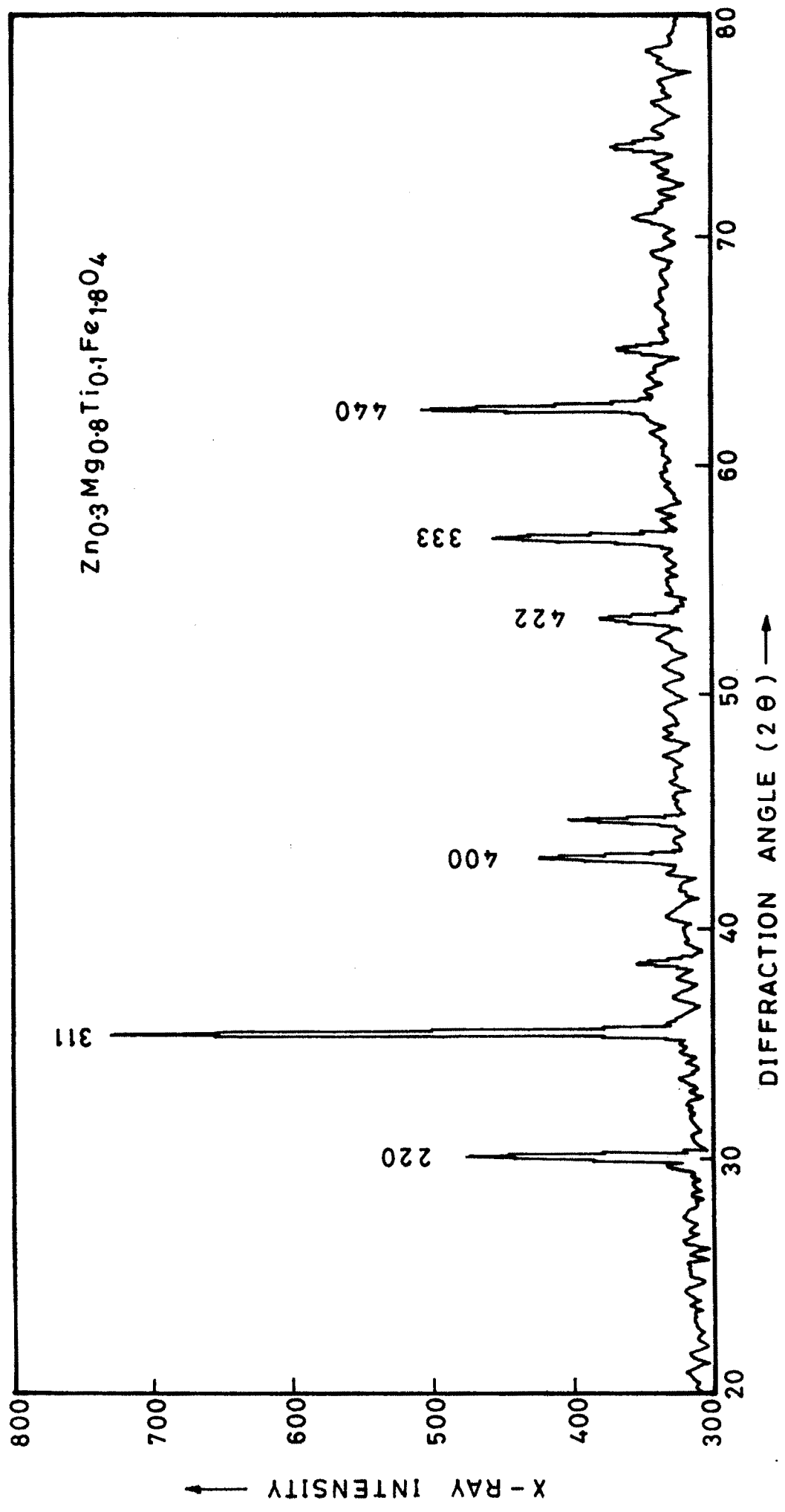


FIG.2.5- X - RAY DIFFRACTION PATTERN OF  $Zn_{0.3}Mg_{0.8}Ti_{0.1}Fe_{1.8}O_4$  .

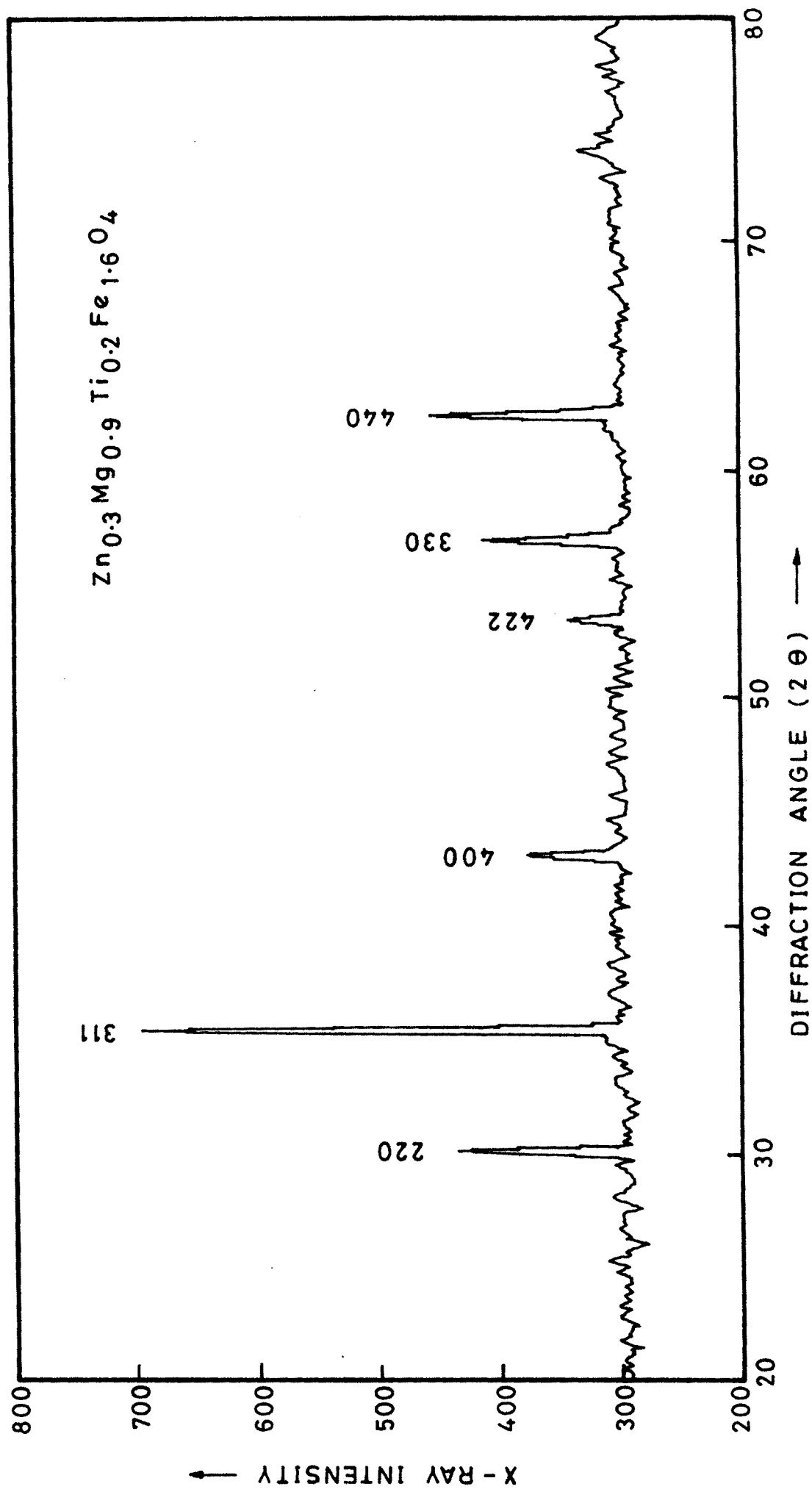


FIG. 2.6 - X - RAY DIFFRACTION PATTERN OF  $Zn_{0.3}Mg_{0.9}Ti_{0.2}Fe_{1.6}O_4$  .

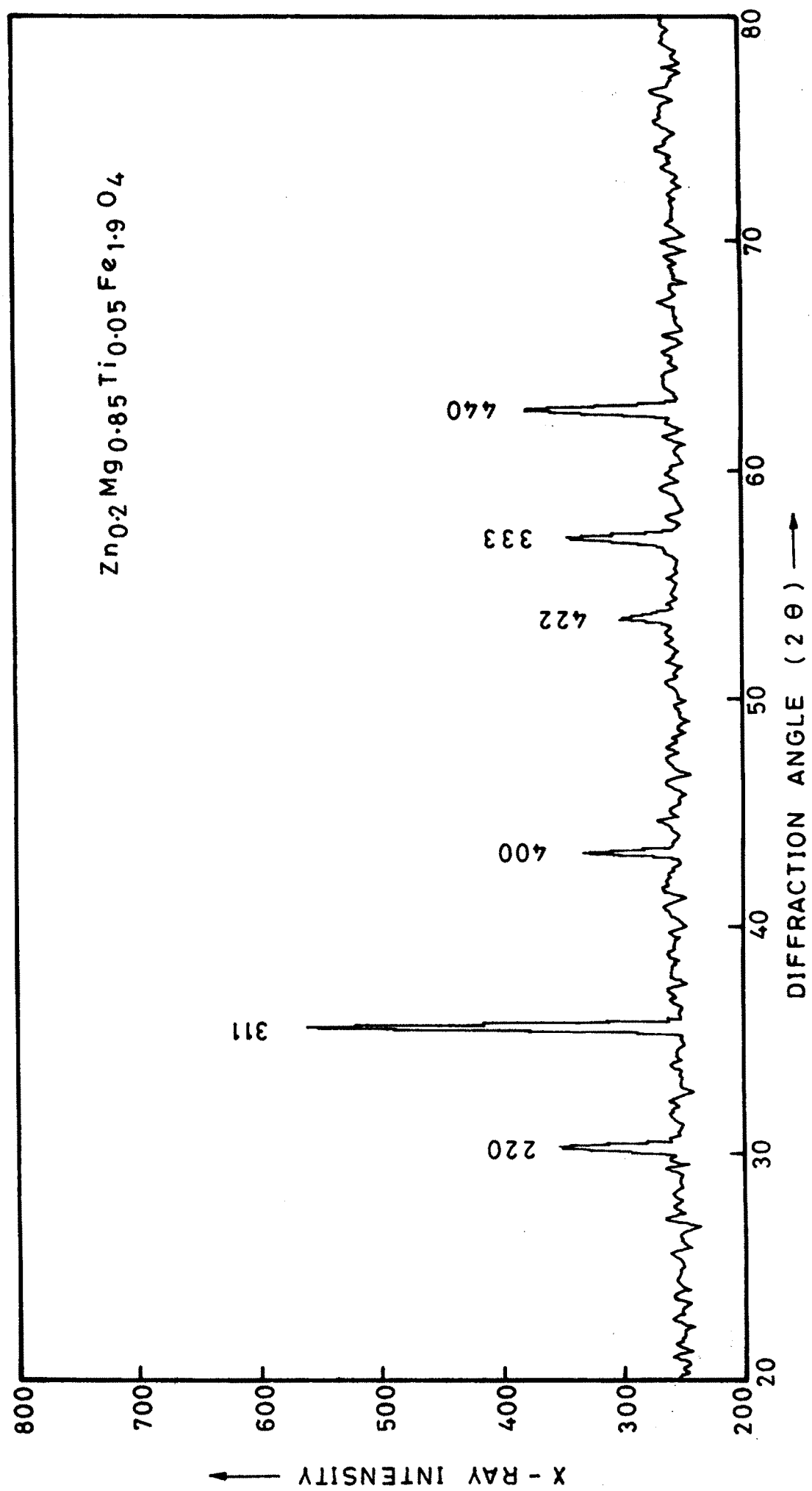


FIG. 2.7 - X-RAY DIFFRACTION PATTERN OF  $Zn_{0.2}Mg_{0.85}Ti_{0.05}Fe_{1.9}O_4$ .

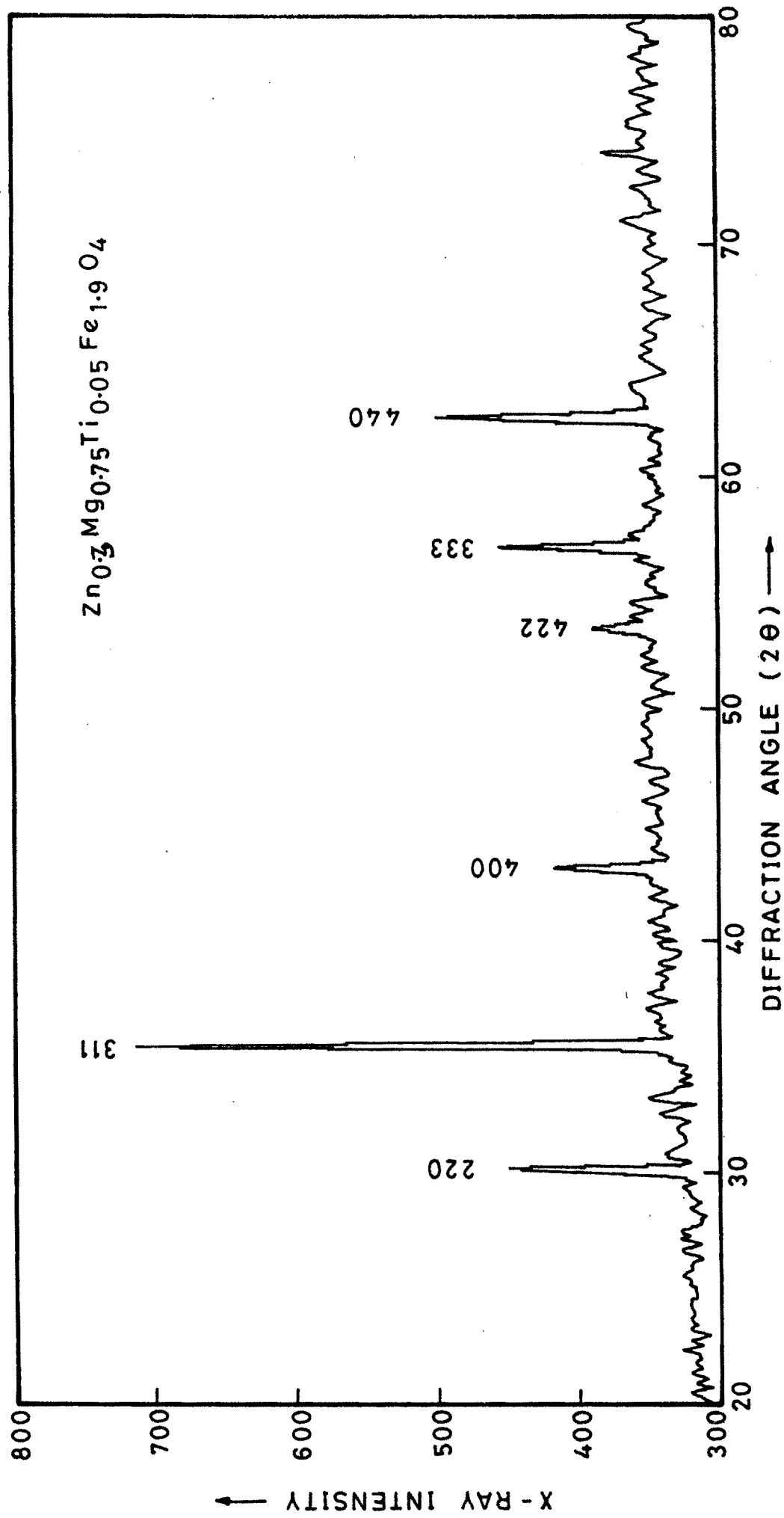


FIG. 2.8 - X - RAY DIFFRACTION PATTERN OF  $Zn_{0.7}Mg_{0.75}Ti_{0.05}Fe_{1.9}O_4$  .

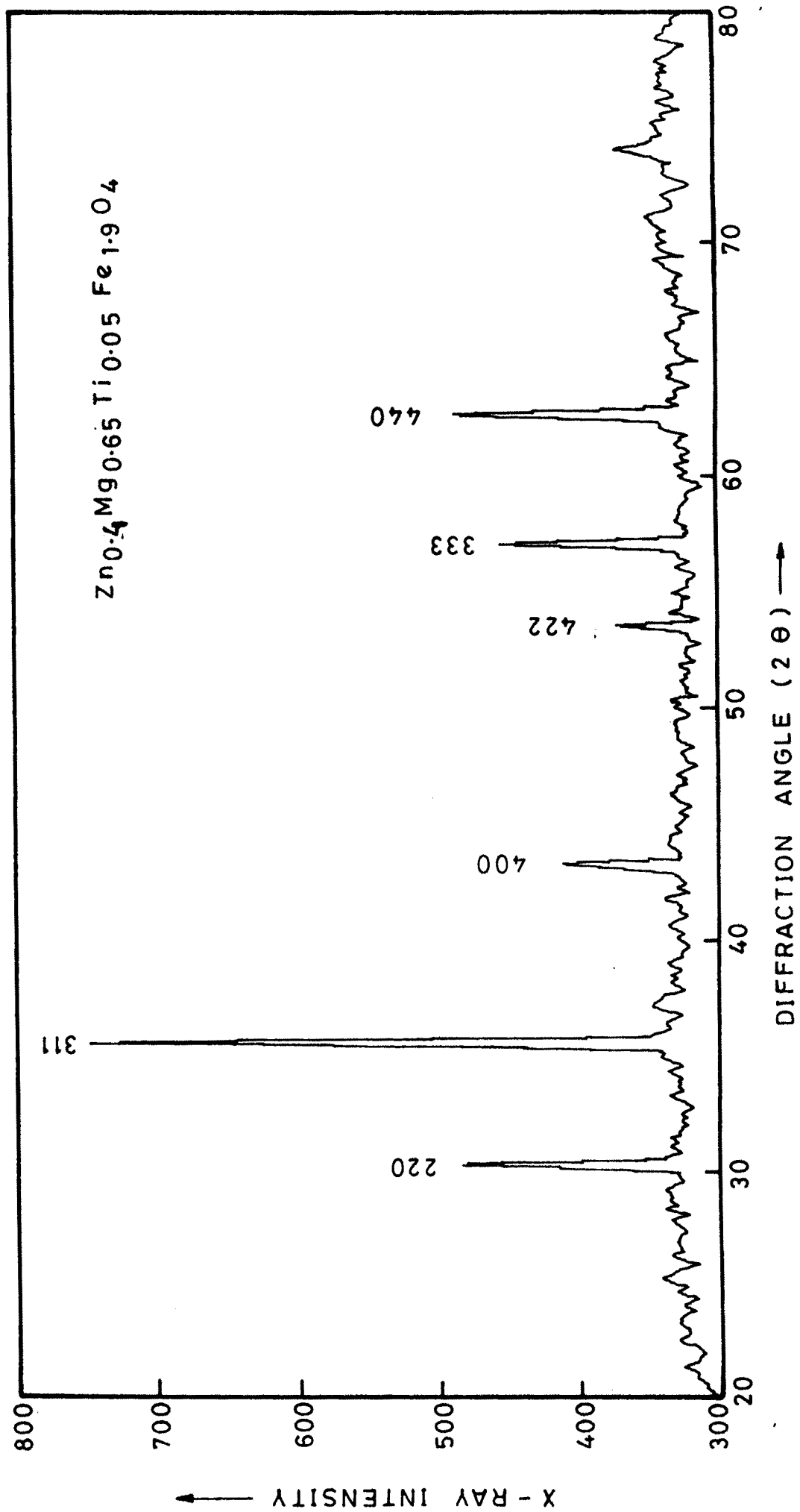


FIG. 2.9 - X - RAY DIFFRACTION PATTERN OF  $Zn_{0.4}Mg_{0.65}Ti_{0.05}Fe_{1.9}O_4$

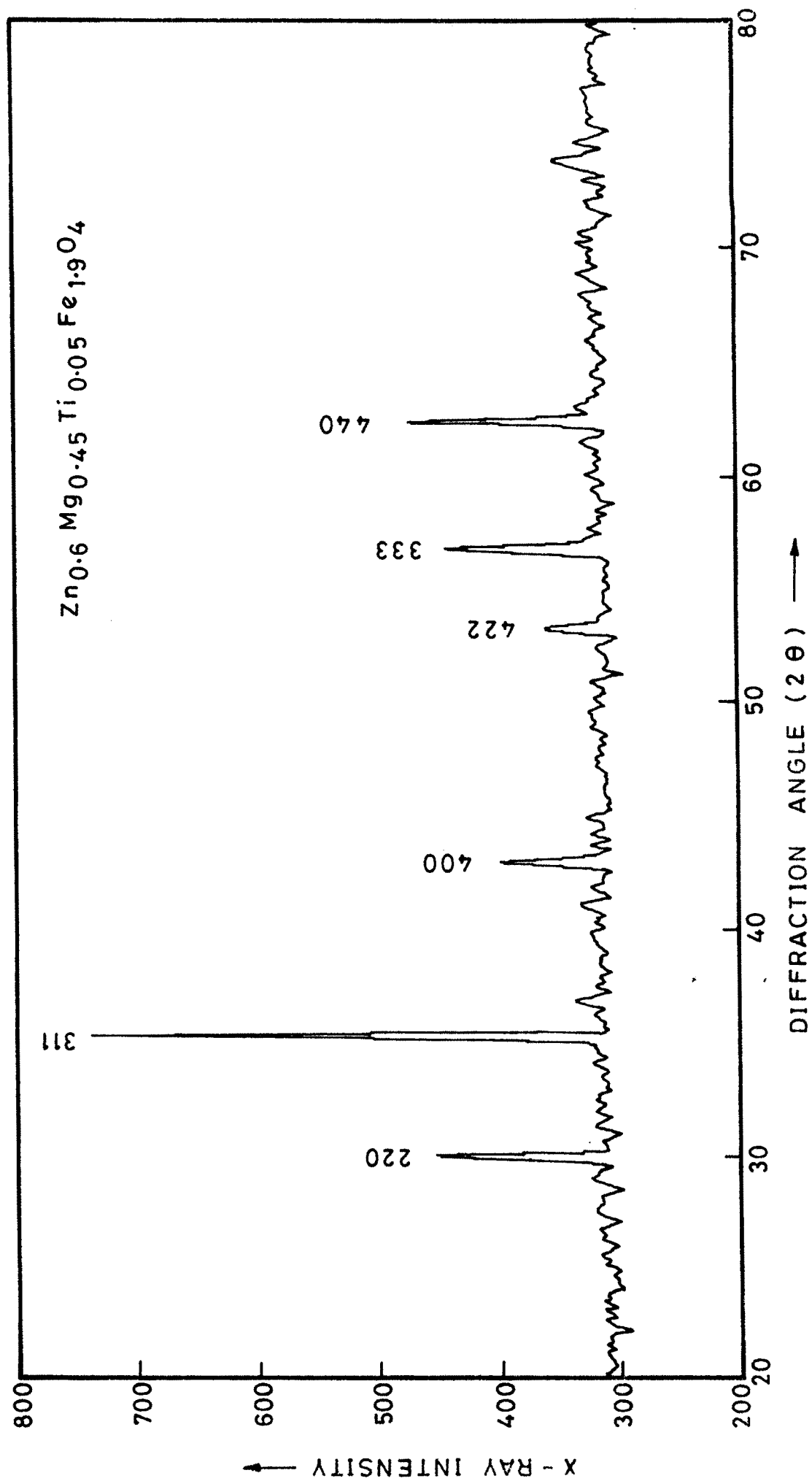


FIG. 2.10 - X-RAY DIFFRACTION PATTERN OF  $Zn_{0.6}Mg_{0.45}Ti_{0.05}Fe_{1.9}O_4$ .

**Table 2.1**

X-ray diffraction data of  $Zn_{0.3}Mg_{0.7}Fe_2O_4$  ferrite  
Wavelength -  $1.5418 \text{ \AA}$   
lattice parameter a -  $8.38 \text{ \AA}$   
Structure - Cubic

Sr. No.	$2\theta$ , deg	$d_{calc}$ , $\text{\AA}$	$d_{obs}$ , $\text{\AA}$	(hkl)
1	30.10	2.9664	2.9664	220
2	35.45	2.5296	2.5298	311
3	43.14	2.0975	2.0953	400
4	53.42	1.7126	1.7136	422
5	57.55	1.6146	1.6001	333
6	62.50	1.4831	1.4847	440

**Table 2.2**

X-ray diffraction data of  $Zn_{0.3}Mg_{0.7}Ti_{0.05}Fe_{1.95}O_4$  ferrite  
Wavelength -  $1.5418 \text{ \AA}$   
lattice parameter a -  $8.38 \text{ \AA}$   
Structure - Cubic

Sr. No.	$2\theta$ , deg	$d_{calc}$ , $\text{\AA}$	$d_{obs}$ , $\text{\AA}$	(hkl)
1	30.10	2.9627	2.9666	220
2	35.47	2.5266	2.5288	311
3	43.08	2.0950	2.0978	400
4	53.47	1.7105	1.7123	422
5	56.95	1.6127	1.6155	333
6	62.55	1.4813	1.4838	440

**Table 2.3**

X-ray diffraction data of  $Zn_{0.3}Mg_{0.9}Ti_{0.1}Fe_{1.6}O_4$   
ferrite  
Wavelength - 1.5418 Å  
lattice parameter a - 8.39 Å  
Structure - Cubic

Sr. No.	2θ, deg	d <sub>calc</sub> , Å	d <sub>obs</sub> , Å	(hkl)
1	30.07	2.9700	2.9690	220
2	35.41	2.5326	2.5329	311
3	43.00	2.1007	2.1015	400
4	53.38	1.7146	1.7148	422
5	56.91	1.6166	1.6167	333
6	62.65	1.4849	1.4815	440

**Table 2.4**

X-ray diffraction data of  $Zn_{0.3}Mg_{0.9}Ti_{0.2}Fe_{1.6}O_4$   
ferrite  
Wavelength - 1.5418 Å  
lattice parameter a - 8.39 Å  
Structure - Cubic

Sr. No.	2θ, deg	d <sub>calc</sub> , Å	d <sub>obs</sub> , Å	(hkl)
1	30.14	2.9663	2.9622	220
2	35.45	2.5296	2.5298	311
3	43.09	2.0975	2.0976	400
4	53.45	1.7126	1.7129	422
5	56.93	1.6146	1.6162	333
6	62.51	1.4838	1.4845	440

**Table 2.5**

X-ray diffraction data of  $Zn_{0.2}Mg_{0.05}Ti_{0.05}Fe_{1.9}O_4$   
ferrite  
Wavelength - 1.5418 Å  
lattice parameter a - 8.35 Å  
Structure - Cubic

Sr. No.	2θ, deg	$d_{calc}$ , Å	$d_{obs}$ , Å	(hkl)
1	30.23	2.9521	2.9536	220
2	35.60	2.5176	2.5195	311
3	43.21	2.0875	2.0918	400
4	53.55	1.7061	1.7099	422
5	57.09	1.6069	1.6120	333
6	62.65	1.4760	1.4817	440

**Table 2.6**

X-ray diffraction data of  $Zn_{0.3}Mg_{0.75}Ti_{0.05}Fe_{1.9}O_4$   
ferrite  
Wavelength - 1.5418 Å  
lattice parameter a - 8.38 Å  
Structure - Cubic

Sr. No.	2θ, deg	$d_{calc}$ , Å	$d_{obs}$ , Å	(hkl)
1	30.10	2.9626	2.9666	220
2	35.47	2.5266	2.5288	311
3	43.08	2.0950	2.0978	400
4	53.47	1.7105	1.7123	422
5	56.95	1.6127	1.6155	333
6	62.55	1.4813	1.4838	440

**Table 2.7**

X-ray diffraction data of  $Zn_{0.4}Mg_{0.65}Ti_{0.05}Fe_{1.9}O_4$   
ferrite

Wavelength - 1.5418 Å  
lattice parameter a - 8.36 Å  
Structure - Cubic

Sr. No.	2θ, deg	d <sub>calc</sub> , Å	d <sub>obs</sub> , Å	(hkl)
1	30.24	2.9560	2.9257	220
2	35.58	2.5206	2.5209	311
3	43.19	2.0901	2.0927	400
4	53.59	1.7064	1.7086	422
5	57.04	1.6088	1.6132	333
6	62.62	1.4778	1.4823	440

**Table 2.8**

X-ray diffraction data of  $Zn_{0.4}Mg_{0.45}Ti_{0.05}Fe_{1.9}O_4$   
ferrite

Wavelength - 1.5418 Å  
lattice parameter a - 8.42 Å  
Structure - Cubic

Sr. No.	2θ, deg	d <sub>calc</sub> , Å	d <sub>obs</sub> , Å	(hkl)
1	29.91	2.9804	2.9845	220
2	35.27	2.5417	2.5426	311
3	42.87	2.1075	2.1076	400
4	53.22	1.7207	1.7196	422
5	56.76	1.6223	1.6205	333
6	62.35	1.4902	1.4881	440

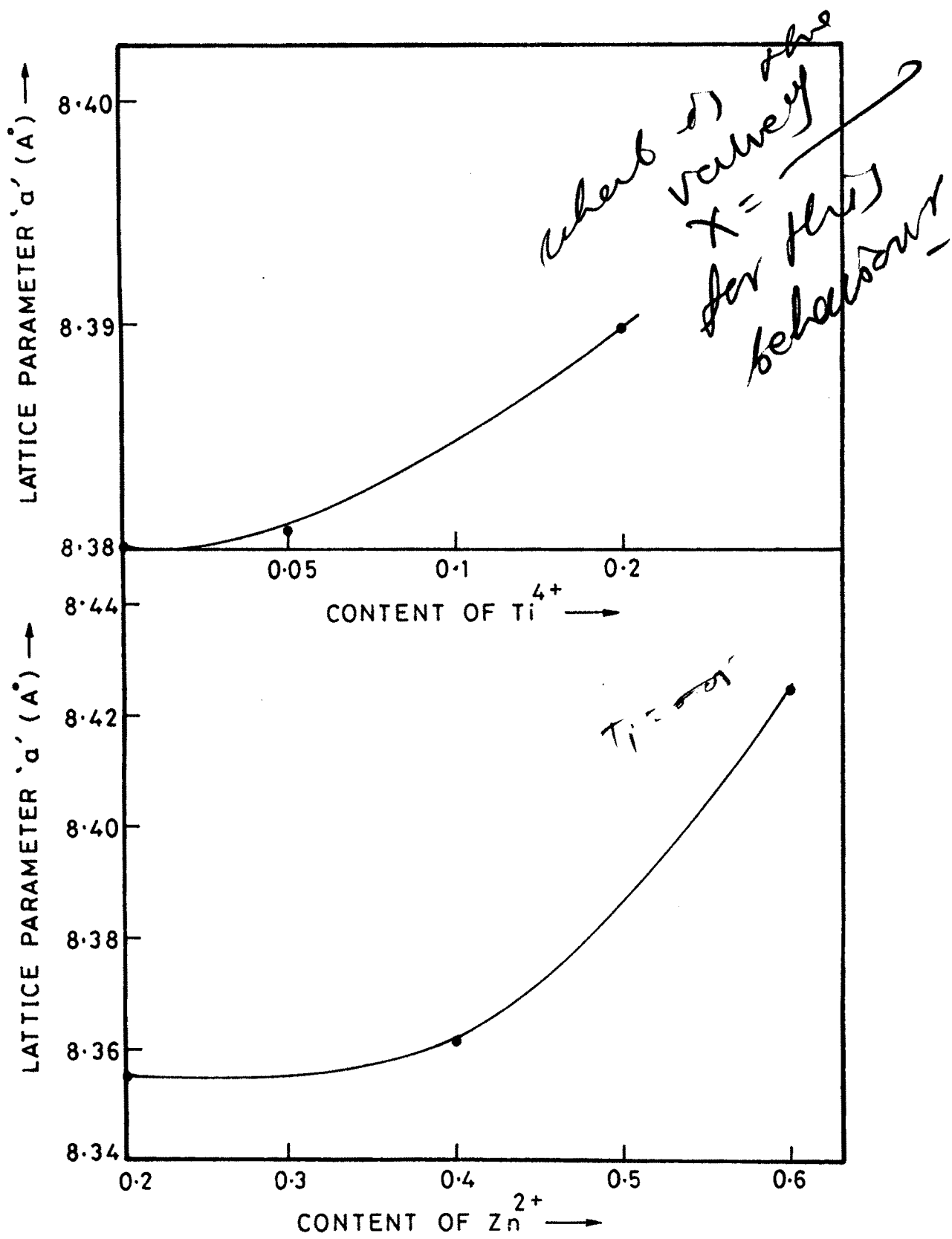


FIG. VARIATION OF LATTICE PARAMETER WITH CONTENT OF  $Ti^{4+}$  &  $Zn^{2+}$ .

content of  $\text{Sn}^{4+}$  and  $\text{Zn}^{2+}$ . It is found that the lattice parameter increases with the increase of  $\text{Sn}^{4+}$  and  $\text{Zn}^{2+}$  content. Similar results have also been reported in case of  $\text{Ti}^{4+}$  substituted nickel zinc ferrites by Baijal et al [16].

$T_i = f$

Figure 2.11b shows the compositional variation of lattice parameter for the series  $\text{Zn}_x\text{Mg}_{1-x+t}\text{Ti}_t\text{Fe}_{2-2t}\text{O}_4$  where  $t = 0.05, x = 0.2, 0.3, 0.4, 0.6$ . The observed increase in the lattice parameter on addition of  $\text{Zn}^{2+}$  in the system can be attributed to the ionic volume differences ( $\text{Zn}^{2+}$  ( $0.80 \text{ \AA}$ ) and  $\text{Mg}^{2+}$  ( $0.75 \text{ \AA}$ )). The role of  $\text{Zn}^{2+}$  ions is to occupy A-site and to increase the lattice parameter. Small amount of  $\text{Ti}^{4+}$  does not appear to distort the lattice parameter in case of Mg or Zn ferrite.

The bond lengths ( $R_A$  and  $R_B$ ) and site radii ( $r_A$  and  $r_B$ ) calculated using the following relations are given in Tables 2.9 and 2.10.

$$\begin{aligned} R_A &= a \sqrt{3} (\delta + 1/8) \\ \text{and} \quad R_B &= a \sqrt{1/16 - \delta/2 + 3\delta^2} \end{aligned} \quad \dots \quad 2.2$$

$$\begin{aligned} r_A &= (u - 1/4) a \sqrt{3} - R_A \\ \text{and} \quad r_B &= (5/8 - u) a - R_B \end{aligned} \quad \dots \quad 2.3$$

where  $R_A$  = Distance of cations from oxygen

**Table - 2.9**

Data on bond lengths ( $R_A$ ,  $R_B$ ) and site radii ( $r_A$ ,  $r_B$ ) for  $Zn_xMg_{1-x+t}Ti_tFe_{2-2t}O_4$  ( where  $x = 0.3$  ) ferrites

t	$R_A$ , Å	$R_B$ , Å	$r_A$ , Å	$r_B$ , Å
0.0	1.9304	2.0296	0.5804	0.6779
0.05	1.9304	2.0296	0.5804	0.6779
0.1	1.9350	2.0344	0.5938	0.6815
0.2	1.9350	2.0320	0.5827	0.6803

**Table - 2.10**

Data on bond lengths ( $R_A$ ,  $R_B$ ) and site radii ( $r_A$ ,  $r_B$ ) for  $Zn_xMg_{1-x+t}Ti_tFe_{2-2t}O_4$  ( where  $t = 0.05$  ) ferrites

x	$R_A$ , Å	$R_B$ , Å	$r_A$ , Å	$r_B$ , Å
0.2	1.9246	2.0230	0.5746	0.6719
0.3	1.9304	2.0296	0.5804	0.6779
0.4	1.9301	2.0247	0.5758	0.6731
0.6	1.9419	2.0417	0.5908	0.6888

$R_B$  = Distance of anions from oxygen in B site

$R_O$  = Radius of oxygen ion = 1.35 Å

$r_A$  = Tetrahedral site radius

$r_B$  = Octahedral site radius

$\delta$  = Deviation from oxygen parameter (u)

= u -  $U_{ideal}$  [  $U_{ideal}$  = 0.375 Å ]

From Tables 2.9 and 2.10 it is seen that the bond length  $R_B$  is always greater than  $R_A$ . There is no remarkable change in the bond lengths and site radii of the samples.

The x-ray density ( $d_x$ ) and actual density ( $d_a$ ) and porosity (P) of the samples were calculated from the relations -

$$d_x = \frac{8M}{Na^3} \quad \dots \quad 2.4$$

$$d_a = \frac{m}{\pi r^2 t} \quad \dots \quad 2.5$$

$$\text{and } P(\%) = (d_x - d_a) / d_x * 100 \quad \dots \quad 2.6$$

where M = Molecular weight of sample

N = Avogadro's Number

a = lattice parameter

m = mass of pellet

r = radius of pellet

**Table 2.11**

X-ray density, actual density and porosity data for  
 $Zn_xMg_{1-x+t}Ti_tFe_{2-2t}O_4$  ( where  $x = 0.3$  ) ferrites

t	$d_{x-ray}(dx)$ gm/cc	$d_{actual}(da)$ gm/cc	porosity, % (P)
0.0	4.79	2.84	40.52
0.05	4.74	2.57	45.78
0.1	4.67	2.69	42.35
0.2	4.59	2.71	40.90

**Table 2.12**

X-ray density, actual density and porosity data for  
 $Zn_xMg_{1-x+t}Ti_tFe_{2-2t}O_4$  ( where  $t = 0.05$  ) ferrites

x	$d_{x-ray}(dx)$ gm/cc	$d_{actual}(da)$ gm/cc	porosity, % (P)
0.2	4.69	2.75	41.23
0.3	4.74	2.57	45.78
0.4	4.87	3.01	38.18
0.6	3.49	3.15	35.25

t = thickness of pellet

Data on x-ray density, actual density and porosity is given in Tables 2.11 and 2.12. The samples are about 40% porous.

## SECTION - C

### INFRA-RED SPECTRA

#### 2.8 INTRODUCTION

Electromagnetic radiation with wavelengths in the range 1 micron to 1 mm is termed as infrared radiation. The energy corresponds to the vibrational modes of molecular motion. Therefore the vibrational energy of the molecules in the solids is determined by infrared spectroscopy.

The optical spectra of ferrites give information about the various vibrational modes in the presence or absence of  $Fe^{2+}$  ions in the ferrites, where as the vibrational, electronic and magnetic dipole spectra provide information about the position and valency of the ions in the crystal. Infrared spectra are used to detect the presence of absorption or emission bands in the ferrites.

Waldron [17] has studied infrared spectra of some simple ferrites in the range of  $100\text{ cm}^{-1}$  to  $1000\text{ cm}^{-1}$ .

bands

He has observed two absorption bands in the frequency range of  $200 \text{ cm}^{-1}$  to  $1000 \text{ cm}^{-1}$ . He has assigned the high frequency band ( $\nu_1$ ) at  $600 \text{ cm}^{-1}$  to tetrahedral complexes and low frequency band ( $\nu_2$ ) at  $400 \text{ cm}^{-1}$  to octahedral complexes. He also reported that a gradual increase in the absorption of higher frequencies caused by electronic transition. Hafner [18], Tarte [19] and others [20,21] applied infrared spectroscopy to investigate the absorption bands in many normal as well as inverse spinel ferrites. It has been pointed out that vibrational frequencies depend on the mass of cations, bonding force, distance and unit cell dimensions [22]. Hafner [18], White and Angelish [21] and many other workers [19,22,23,24] have studied the IR bands in the ferrites and their conclusions were the same as those of Waldron. The bands  $\nu_3$  and  $\nu_4$  are sometimes observed in spinel ferrites [25].

For the analysis of an IR spectrum, it is necessary to consider a vibrational problem, which is most conveniently treated by classifying the crystals according to the continuity of bonding as (I) continuously bonded, (II) discontinuously bonded and (III) intermediates.

In the continuously- bonded crystals the atoms are bonded to all the nearest neighbours by the equivalent forces (ionic, covalent or van der Waals) and frequency distribution of the vibration is given by Debye or Born-van Karman treatment of classical mechanical problem and includes simple ionic crystals.

In the discontinuously bonded crystals, sets of atoms are tightly bonded by (intermolecular) chemical valence forces and separated from adjacent sets by weak van der Waals forces. e.g. solid polyatomic gases, most organic compounds, non metallic compounds.

In the third class, the intermolecular forces are somewhat greater than those in molecular cases and the branches may overlap and the vibrational problem may occasionally be treated as a perturbation of class-2 cases. Examples of this group includes ionic crystals containing polyatomic ions, hydrogen-bonded crystals and strongly dipolar crystals.

The application of I.R spectroscopy to ferrites is mainly to -

- 1) detect the completion of solid state reaction
- 2) study of cation distribution
- 3) study the deformation of cubic spinel structure and distribution of cations and

4) calculate force constants for tetrahedral and octahedral sites.

## 2.9 EXPERIMENTAL TECHNIQUES

The IR spectra of all ferrite samples were recorded on Perkin Elmer IR spectrometer (Model 783). For recording the spectra, powders were mixed with KBr in the ratio of 1:25 by weight to ensure uniform dispersion in the KBr pellet. The mixed powders were pressed in a cylindrical die to obtain clean discs of approximately 1 mm thickness. The IR spectra in the frequency range  $200-800\text{ cm}^{-1}$  were recorded at room temperature. This facility is made available by USIC, Shivaji University, Kolhapur.

## 2.10 RESULTS AND DISCUSSION

The IR spectra of present samples are shown in Figures 2.12 to 2.15. The spectra were used to locate the band positions which are noted in Tables 2.13 and 2.14. In general the present ferrite samples show two absorption bands  $\nu_1$  and  $\nu_2$ . The high frequency band ( $\nu_1$ ) has been assigned to tetrahedral complexes while the low frequency band ( $\nu_2$ ) to the octahedral complexes.

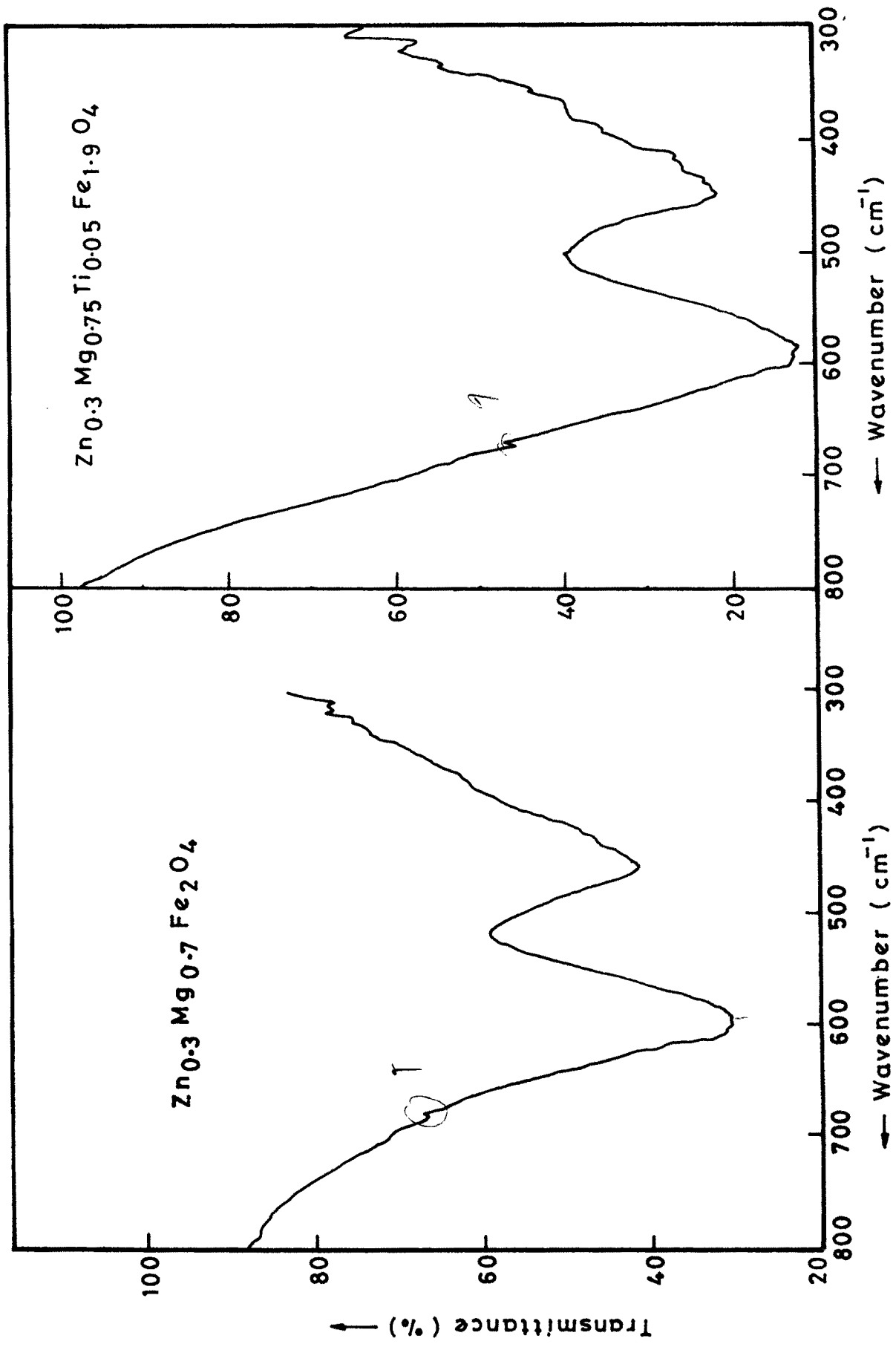


FIG. 2.12.- IR SPECTRA OF  $Zn_{0.3}Mg_{0.7}Fe_2O_4$  &  $Zn_{0.3}Mg_{0.75}Ti_{0.05}Fe_{1.9}O_4$



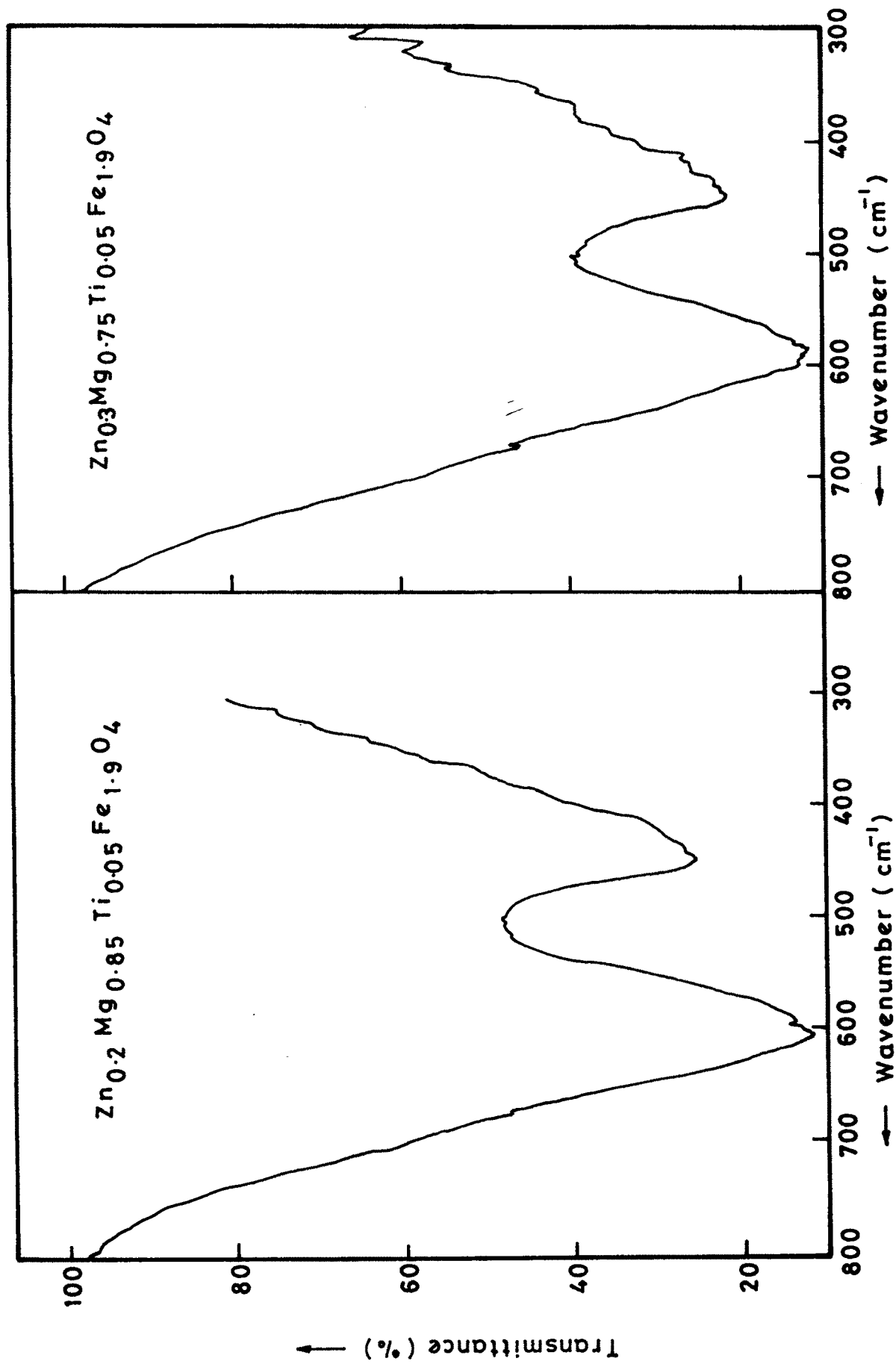


FIG. 2-14 — IR SPECTRA OF  $Zn_{0.2}Mg_{0.85}Ti_{0.05}Fe_{1.9}O_4$  &  $Zn_{0.3}Mg_{0.75}Ti_{0.05}Fe_{1.9}O_4$

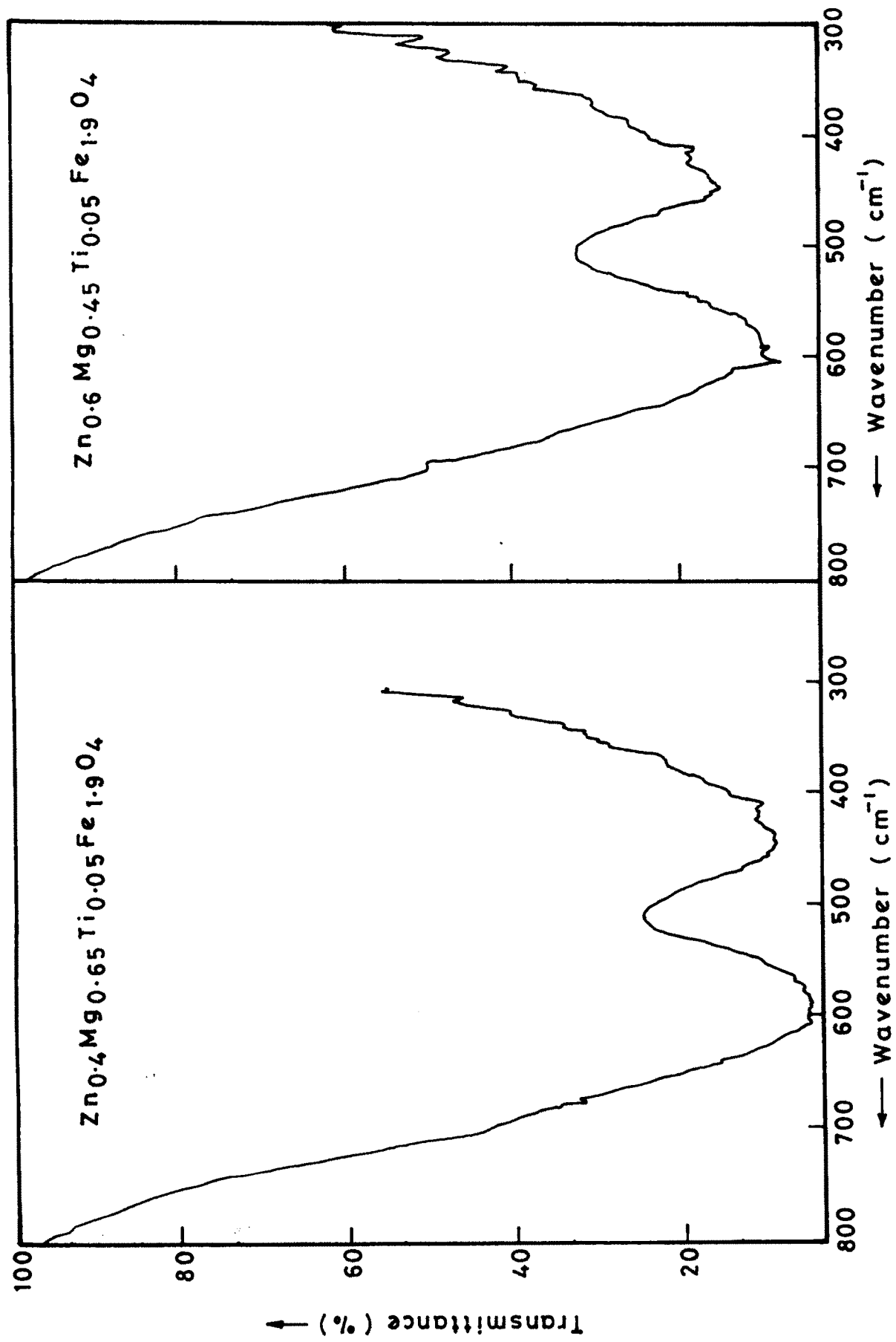


FIG. 2.13 - IR SPECTRA OF  $Zn_{0.4}Mg_{0.65}Ti_{0.05}Fe_{1.9}O_4$  &  $Zn_{0.6}Mg_{0.45}Ti_{0.05}Fe_{1.9}O_4$

Table 2.13

Lattice vibration frequencies for  $Zn_xMg_{1-x+t}Ti_tFe_{2-2t}O_4$  ferrites ( $x = 0.3$ )

t	1, $cm^{-1}$	2, $cm^{-1}$
0.0	590	445
0.05	583	449
0.1	602	452
0.2	600	451

Table 2.14

Lattice vibration frequencies for  $Zn_xMg_{1-x+t}Ti_tFe_{2-2t}O_4$  ferrites ( $t = 0.05$ )

x	1, $cm^{-1}$	2, $cm^{-1}$
0.2	590	442
0.3	583	449
0.4	604	445
0.6	602	450

In the present study the absorption band for the series are found to be in the expected range (600-400  $\text{cm}^{-1}$ ). The difference in  $\nu_1$  and  $\nu_2$  is expected due to the different Fe-O distances at the octahedral and tetrahedral sites. The Table 2.13<sup>2.14</sup> reveals that the positions of absorption bands change slightly from one mixed ferrite to other. This change may be due to the change in the  $\text{Fe}^{3+}-\text{O}_2^-$  complexes with the increase of zinc concentration. It suggests that the method of preparation, grain size and porosity can be the influencing factors in locating the positions. The band positions in the present system are not very regular. // 9

Braber [26] has classified the lattice vibrations of the cubic spinel. According to his classification there are four IR active modes which are triply degenerate vibrations may split in two or three vibrations for normal spinels. If the splitting is not too large and there is certain statistical distribution of various cations over the tetrahedral and octahedral sites. One cannot observe the splitting but only broadening of the absorption. The broad absorption bands which are observed in the spectra of present system may be due to this effect because the Mg ferrite is a partially inverse whereas Zn ferrite is normal

ferrite [27]. The  $Ti^{4+}$  ions are distributed both over the A and B-sites.

## REFERENCES

1. Economus G.  
J. Amer. Ceram. Soc. 38 (1955) 241
2. Wolf W. P. & Rodrigue G.P.  
J. Appl. Phys. 29 (1958) 105
3. Wagner C.  
Z. Phy. Chem. B-34 (1936) 309
4. Carter R.E.  
J. Am. Ceram. Soc. , 44 ( 1961 ) 611
5. Reingen P.  
"Science of Ceramics"  
Stewart (ed.) vol-3 Academic Press, N.Y. (1967)
6. Kooy C.  
"Material Transport in Solid State Reaction"  
Fifth Int. Symp. on Reactivity Solids, Munich  
(1964) p-21-28, Elsevier Amsterdam (1965)
7. Murray P., Livey D. T. & Williams J.  
"Ceramic Fabrication Processes"  
W. D. Kingery (Ed.),  
Wiley, New York (1958) 147
8. Oudemans G.J. and Gruintises G.S.  
Ceram. Bull. (1966) 411
9. Debye P. and Scherrer P.  
Physic 17 (1916) 277 and 18 (1917) 219
10. Hull A.N.  
Phy. Rev. 9 (1916) 564 and 10 (1917) 661
11. Shull C.G., Wollan E.O. & Koehler W.C.  
Phys. Rev. 84 (1952) 912
12. Hastings J.M. & Corliss L.M.  
Rev. Mod. Phys. 25 (1953) 114
13. Suresh K., Kumar N.R.S. and Patil K.G.  
Advances in Materials (1991)

14. Das A.R., Ananthan V.S. and Khan D.C.  
J. Appl. Phys. 57(1), (1985)
15. Vershney Usha, Churchill R.J., Puri R.K. and  
Mendiratta R.G.  
Proc. ICF (1989) 255
16. Baijal J.S., Kothari Dipika and Pharyoubam Sumitra  
Proc. ICF-5 (1989) 371
17. Waldron R.D.  
Phys. Rev. 99 (1955) 1727
18. Hafner S.T.  
Z. Krist, 115 (1961) 331
19. Tarte P.  
Spectrochim. Acta. 19 (1963) 49
20. Freudhomme J.  
Spectrochim. Acta. 26-A (1970) 985
21. White R.B. and De Angelish B.A.  
Spectrochim. Acta. 23-A (1963) 985
22. Murthy V.R.K., Chitrasankar S., Reddy K.V. and  
Sobhanadri J.  
Ind. J. of Pure and Applied Phys., 36 (1978) 79
23. Pakhomova N.L. and Christopher V.  
Phys. Stat. Solidi, (a) 105 (1987) 543
24. Reddy P. V. and Salagram M.  
Phys. Stat. Solidi (a) 100 (1987) 639
25. Satomi K.J.  
Phys. Soc. Japan 16 (1961) 258
26. Brabers V.A.M.  
Phys. Stat. Solidi (a) 33 (1969) 563
27. Srinivasan T.T., Srivastava C.M., Venkatramani N.  
and Patni M.J.  
Bull. Mater. Sci, vol. 6, no. 6 (1984) 1063